Vacuum ultraviolet and near-infrared excited luminescence properties of $Ca_3(PO_4)_2:RE^{3+}$, Na^+ (RE=Tb, Yb, Er, Tm, and Ho)

Jia Zhang [a], Yuhua Wang [a,*], Linna Guo [a], Feng Zhang [a], Yan Wen [a], Bitao Liu [a], Yan Huang [b]

[a] Department of Material Science, School of Physical Science and Technology, Lanzhou University, Lanzhou 730000, PR China
[b] Laboratory of Beijing Synchrotron Radiation, Institute of High Energy Physics, Chinese Academy of Sciences, Beijing 100049, PR China

ABSTRACT

Tb^{3+}, Yb^{3+}, Tm^{3+}, Er^{3+}, and Ho^{3+} doped $Ca_3(PO_4)_2$ were synthesized by solid-state reaction, and their luminescence properties were studied by spectra techniques. Tb^{3+}-doped samples can exhibit intense green emission under VUV excitation, and the brightness for the optimal Tb^{3+} content is comparable with that of the commercial $Zn_2SiO_4:Mn^{2+}$ green phosphor. Under near-infrared laser excitation, the upconversion luminescence spectra of Yb^{3+}, Tm^{3+}, Er^{3+}, and Ho^{3+} doped samples demonstrate that the red, green, and blue tricolored fluorescence could be obtained by codoping Yb^{3+}–Ho^{3+}, Yb^{3+}–Er^{3+}, and Yb^{3+}–Tm^{3+} in $Ca_3(PO_4)_2$, respectively. Good white upconversion emission with CIE chromaticity coordinates (0.358, 0.362) is achieved by quadri-doping Yb^{3+}–Tm^{3+}–Er^{3+}–Ho^{3+} in $Ca_3(PO_4)_2$, in which the cross-relaxation process between Er^{3+} and Tm^{3+}, producing the $^1D_2$–$^3F_4$ transition of Tm^{3+}, is found. The upconversion mechanisms are elucidated through the laser power dependence of the upconverted emissions and the energy level diagrams.

© 2011 Elsevier Inc. All rights reserved.

1. Introduction

Inorganic luminescence materials have found many practical applications in modern lighting and display fields, such as fluorescence lamps, cathode-ray tubes, field emission displays and plasma display panels (PDPs) [1]. And as a kind of important luminescence material, rare earth (RE) ions doped phosphors have gained much attention in recent years. It is well known that phosphors under vacuum ultraviolet (VUV) excitation are widely used for PDPs and Hg-free lamps, in which the plasma excitation resource containing noble gas mixture mainly provides the Xe resonance emission line (147 nm) and/or the Xe_2 molecular emission band (172 nm) [2–4]. So excellent phosphors for these applications must have broad and strong absorption around 147–172 nm to meet the emission wavelengths of the excitation source. Additionally, for the time being, the interest in three-dimensional (3D) displays has steadily grown due to increasing needs for advanced image devices, for which the 3D PDPs operates using the images that are separated to the left and right eyes by dividing the scanning period [5,6]. This 3D device requires higher brightness and shorter response time than the conventional PDPs. However, the commercial $Zn_2SiO_4:Mn^{2+}$ currently used for the green phosphor in PDPs suffers not only low luminous efficiency, but also a long decay time, which would result in a cross talk between images and deterioration of image quality. Hence, it is essential to develop intense-emitting and fast-decaying PDP phosphors.

Upconversion (UC) as a process where low-energy light, usually near-infrared (NIR) or infrared, is converted to higher energies, ultraviolet (UV) or visible (VIS), via multiple absorptions or energy transfers (ETs) [7,8], has been also focused on due to its promising applications on solid-state lasers, solar cells, biological fluorescence labels and so on [9]. Generally speaking, the most used activator ions in UC phosphors to generate red, green, and blue fluorescence are Ho^{3+}, Er^{3+}, and Tm^{3+} as reported in many Refs. [9–14]. However, these RE ions themselves cannot emit efficiently due to the lack of matched energy levels with the 980 nm photon energy or the low efficiency, and Yb^{3+} as an efficient sensitizer with a large absorption cross section in NIR region is always co-doped to enhance the fluorescence intensities of Ho^{3+}, Er^{3+}, and Tm^{3+} [11,14]. Furthermore, there is also a great interest in the generation of white light sources upon a NIR laser diode (LD) excitation, and the usual way to achieve this is to combine the three fundamental red, green, and blue light colors, which greatly challenges people's ability of material design including host composition and the suitable combination of sensitizers and activator ions [9,14]. So far, the UC luminescence materials are limited to transparent glasses and rarely involve RE doped opaque ceramics. However, opaque ceramics have higher absorption abilities compared to glass materials, and the luminescence efficiency can be enhanced effectively [15].

Tricalcium phosphate $Ca_3(PO_4)_2 \cdot$ (CPO), as an outstanding matrix material, has been investigated much due to oxides are usually very stable chemically, mechanically, and thermally. CPO is the best known as one of the most important biocompatible, and the luminescence properties of RE-doped CPO have been also extensively studied in recent years. For instance, Nagpure et al. [16] reported the

* Corresponding author. Fax: +86 931 8913554.
E-mail address: wyh@lzu.edu.cn (Y. Wang).

photoluminescence and thermoluminescence of Eu^{3+} and Dy^{3+} activated CPO, the thermoluminescence of $CPO:Tm^{3+}$ has been studied by Mizuguchi et al. [17]. In this compound, it is possible to achieve intense green emission upon VUV excitation by doping Tb^{3+} due to the presence of PO_4^{3-}, which usually has strong absorption in the range of 145–160 nm [18,19]. And it is well known that Tb^{3+} possesses a much shorter decay time relative to Mn^{2+}, which is expected to meet the requirements of 3D PDPs. In addition, we also realized red, green, and blue emissions under 980 nm excitation at by co-doping Yb^{3+}–Ho^{3+}, Yb^{3+}–Er^{3+}, and Yb^{3+}–Tm^{3+} in CPO matrix, respectively. And good white light color has been obtained in Yb^{3+}–Ho^{3+}–Er^{3+}–Tm^{3+} quadri-doped CPO.

2. Experimental

Powder samples of RE^{3+} (RE=Tb, Yb, Er, Ho, and Tm) doped CPO were synthesized by a solid-state reaction method. Appropriate amounts of starting materials $CaCO_3$ (99%), $NH_4H_2PO_4$ (99%), Tb_4O_7 (99.99%), Yb_2O_3 (99.99%), Er_2O_3 (99.99%), Ho_2O_3 (99.99%), Tm_2O_3 (99.99%) and $NaCO_3$ (99.8%) were thoroughly mixed in an agate mortar and pre-fired at 600 °C for 3 h in air, then heated at 1150 °C for 8 h in air (for Yb, Er, Ho, and Tm doped samples) or in a reducing atmosphere (5% H_2–95% N_2, for Tb doped samples). Na^+ provided by $NaCO_3$ was used as compensator for charge defects resulting from Ca^{2+} substituted by Ln^{3+}.

The phase purity was determined using a Rigaku D/MAX-2400 powder X-ray diffractometer (XRD) with Cu $K\alpha$ radiation (λ=1.54178 Å) operating at 40 kV and 60 mA. Optical absorption spectra were obtained by a UV/VIS spectrophotometer (Perkin-Elmer Lambda 950) using $BaSO_4$ as a reference in the range of 400–1100 nm. The VUV–UV photoluminescence (PL) and photoluminescence excitation spectra were measured at the VUV spectroscopy station on beam line 4B8 of Beijing Synchrotron Radiation Facility (BSRF), Institute of High Energy Physics. The UC PL spectra were measured using the 980 nm LD as excitation source, with the HORIBA Jobin Yvon Fluorlog-3 Spectrofluorometer system. All the spectra measurements were performed at room temperature in the air.

3. Results and discussion

The XRD patterns of $Ca_{3-2x}(PO_4)_2$:xTb^{3+}, xNa^+ (CPO:xTb^{3+}, xNa^+) ($0.05 \leq x \leq 0.45$) are presented in Fig. 1. All the diffraction
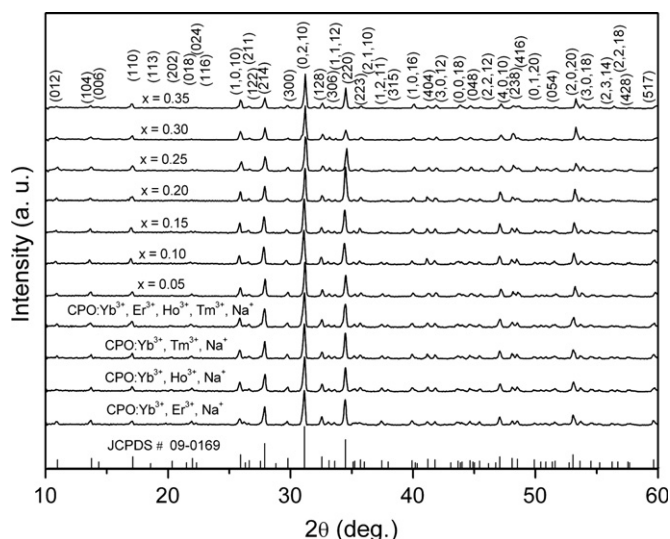
Fig. 1. XRD patterns of CPO:xTb^{3+}, xNa^+ ($0.05 \leq x \leq 0.45$); CPO:$0.15Yb^{3+}$, $0.03Er^{3+}$, $0.18Na^+$; CPO:$0.15Yb^{3+}$, $0.03Ho^{3+}$, $0.18Na^+$; CPO:$0.15Yb^{3+}$, $0.006Tm^{3+}$, $0.156Na^+$; and CPO:$0.15Yb^{3+}$, $0.03Er^{3+}$, $0.045Ho^{3+}$, $0.005Tm^{3+}$, $0.1895Na^+$.
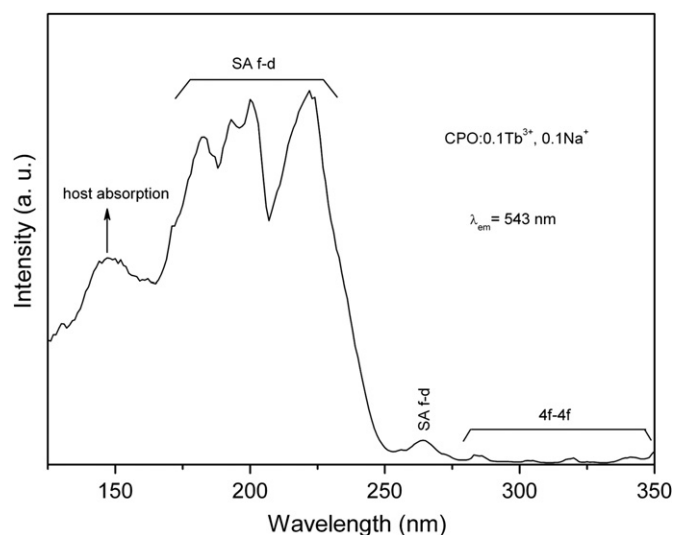
Fig. 2. Excitation spectrum of CPO:$0.1Tb^{3+}$, $0.1Na^+$.

peaks can be indexed to pure hexagonal-structured CPO (JCPDS Card NO.09-0169), indicating the as-prepared samples are single phase.

Fig. 2 shows the excitation spectrum of CPO:$0.1Tb^{3+}$, $0.1Na^+$ by monitoring at 543 nm. According to Ref. [20], the energy levels of tetrahedral PO_4^{3-} molecule have been calculated using the extended Hückel method, which shows the lowest intramolecular transition of $2t_2 \rightarrow 2a$, $3t_2$ exists at 7–10 eV (124–177 nm). And in many VUV phosphors, the absorption position of the PO_4^{3-} has been observed to lie in this region [19,21,22]. Hence, the excitation band between 125 and 165 nm in Fig. 2 could be attributed to the PO_4^{3-} absorption. It is well known that the f–d transition of Ln^{3+} is of broad and strong characteristics, so the strong excitation bands from 165 to 250 nm are assigned to the typical spin-allowed f–d transition of Tb^{3+}, and the weak one around 264 nm could be ascribed to Tb^{3+} spin-forbidden f–d transition. Additionally, some weak $4f$–$4f$ transitions of Tb^{3+} are also observed in the range of 280–350 nm. From this excitation spectrum, it is obvious that Tb^{3+} activated CPO could absorb VUV photons of 147 and 172 nm efficiently, which well matches with the emission wavelength of excitation resource in PDPs or Hg-free lamps.

To study the PL properties of Tb^{3+}-doped CPO upon 147 nm excitation, we measured the emission spectra of a series of CPO:xTb^{3+}, xNa^+ ($0.05 \leq x \leq 0.35$), and the dependence of the Tb^{3+} concentration x on its $^5D_4$–$^7F_5$ emission intensity is shown in the inset (a) of Fig. 3. The optimal Tb^{3+} doping concentration is at x=0.25, so we illustrate the emission spectra of CPO:$0.25Tb^{3+}$, $0.25Na^+$ and the commercial green Zn_2SiO_4:Mn^{2+} both excited at 147 nm in Fig. 3. The four emission peaks centered at 490, 543, 587 and 623 nm of CPO:$0.25Tb^{3+}$, $0.25Na^+$ are attributed to typical $^5D_4$–^7F_J (J=6–3) transitions of Tb^{3+}, but its $^5D_3$–^7F_J transitions disappear, which is due to the enhanced cross relaxation process for large Tb^{3+} doping concentration as described below

$$Tb^3(^5D) + Tb^3(^7F) \rightarrow Tb^3(^5D) + Tb^3(^7F) \qquad (1)$$
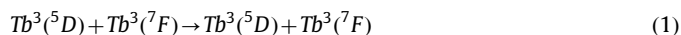
The CPO:$0.25Tb^{3+}$, $0.25Na^+$ has a very strong predominated emission intensity, about 2.5 times stronger than that of Zn_2SiO_4:Mn^{2+}, and exhibits a comparable brightness to Zn_2SiO_4:Mn^{2+} by integrating emission counts from 450 to 650 nm. The inset (b) of Fig. 3 shows the decay curve of $^5D_4$–$^7F_5$ transition (543 nm) of Tb^{3+} in CPO:$0.25Tb^{3+}$, $0.25Na^+$ at 147 nm, which indicates the decay time obtained is 2.53 ms. Hence, the much shorter decay time of Tb^{3+} displays a bigger potential for use in 3D PDPs relative to Zn_2SiO_4:Mn^{2+} (5.22 ms [23]).

Fig. 3. Emission spectra of CPO:0.25Tb^{3+}, 0.25Na$^+$ and commercial green Zn$_2$SiO$_4$:Mn^{2+}, the inset (a) shows dependence of the Tb^{3+} concentration x on the emission intensity of CPO:Tb^{3+}, Na$^+$; the inset (b) shows decay curve of CPO:0.25Tb^{3+}, 0.25Na$^+$.

Fig. 4. Optical absorption spectra of CPO:0.15Yb^{3+}, 0.03Er^{3+}, 0.18Na$^+$; CPO:0.15Yb^{3+}, 0.03Ho^{3+}, 0.18Na$^+$; CPO:0.15Yb^{3+}, 0.006Tm^{3+}, 0.156Na$^+$; and CPO:0.15Yb^{3+}, 0.03Er^{3+}, 0.045Ho^{3+}, 0.005Tm^{3+}, 0.1895Na$^+$.

As discussed above, we have prepared Yb^{3+}, Er^{3+}, Tm^{3+}, and Ho^{3+} doped CPO, and investigated their UC luminescence properties upon NIR LD excitation. The XRD patterns of CPO:RE^{3+}, Na$^+$ (RE=Yb, Er, Tm, and Ho) are shown in Fig. 1. All the diffraction peaks are in good agreement with those of CPO found in the JCPDS card no. 09-0169, indicating the single-phase samples are successfully obtained.

Fig. 4 shows the VIS-NIR absorption spectra of Yb^{3+}, Er^{3+}, Tm^{3+}, and Ho^{3+} doped CPO. All the observed absorption peaks before 850 nm could be attributed to different transitions from the ground states to various excited states of electronic configuration of Er^{3+}, Tm^{3+}, and Ho^{3+} [10]. The extremely strong and broad absorption peaks around 976 nm are assigned to the typical $^2F_{7/2}$–$^2F_{5/2}$ transition of Yb^{3+}, which indicate a large absorption section of Yb^{3+} in NIR region.

Fig. 5 presents the UC emission spectrum of CPO:0.15Yb^{3+}, 0.03Er^{3+}, 0.18Na$^+$ under DL excitation of 980 nm at the pump power of 370 mW. The three emission peaks around 524, 550 and

Fig. 5. UC emission spectrum of CPO:0.15Yb^{3+}, 0.03Er^{3+}, 0.18Na$^+$ under DL excitation of 980 nm, the inset (a) shows dependence of UC emission intensity on excitation powder, the inset (b) shows normalized UC emission spectra by 550 nm at different excitation powers of CPO:0.15Yb^{3+}, 0.03Er^{3+}, 0.18Na$^+$.

668 nm could be attributed to $^2H_{11/2}$–$^4I_{15/2}$, $^4S_{3/2}$–$^4I_{15/2}$ and $^4F_{9/2}$–$^4I_{15/2}$ transitions of Er^{3+}, respectively [24]. To better understand the UC mechanism, the pump power dependence of the UC emissions was measured. For unsaturated UC processes, the number of photons, which are required to populate the upper emitting state can be obtained by the following relation [25]:

$$I_f \propto P^n \tag{2}$$

where I_f is the fluorescent intensity, P is the pump power, and n is the number of photons required to populate the emitting state. For every emission peak at 525, 550 and 668 nm of Er^{3+}, a plot of lnI_f versus P yields a straight line with slope n, as shown in the inset (a) of Fig. 5, and the n values obtained are equal to 1.98, 1.72 and 1.43, respectively. Hence, the three emissions are all two-photon processes. In addition, it is worthwhile to note that the relative intensities among the three emissions are changing under different power excitations, which can be seen from the normalized UC emission spectra by 550 nm in the inset (b) of Fig. 5. It is obvious that the intensity of green emission at 525 nm increases with increasing pump power, however, the red one at 668 nm is opposite to that. The explanation can be combined with the reason for the difference of the obtained n values of the three emission peaks. n values lower than 2 for emissions at 550 and 668 nm could be owing to the following two reasons: (1) Competition between linear decay and UC processes for the depletion of the intermediate excited states [25]. The UC luminescence intensity for an n-photon energy transfer process is proportional to the n-th power of the pump power (P^n) in the limit of infinitely small UC rates, while the intensity is proportional to the pump power (P^1) in the limit of infinitely large UC rates. Hereby, the intensity of an UC luminescence excited by the sequential absorption of n photons has a dependence of P^β on absorbed pump power P, with $1 < \beta < n$. (2) Thermal quenching, which results from the high non-radiative rates at high excitation densities leads to an increase of the temperature in the internal sample, including a thermal effect that leads to the quenching of UC luminescence [26,27]. Since the fitted slope values of n are 1.98, 1.72 and 1.43 for emissions at 525, 550 and 668 nm, respectively, the changing of the emission intensity for 525 nm is more sensitive to pump power compared with that for 550 nm according to Eq. (2), while that of red emission is opposite. In this case, we can confirm that the UC fluorescence color of Yb^{3+}–Er^{3+} co-doped CPO will change with

the excitation pump. Generally, color is represented by color coordinates. So we calculated the chromaticity coordinates from the emission spectra by the method using the 1931 CIE (Commission International de l'Eclairage France) system. The obtained chromaticity coordinates of CPO:0.15Yb^{3+}, 0.03Er^{3+}, 0.18Na$^+$ at the pump powers of 11.6, 63.2, 216, 370 and 480.8 mW are (0.449, 0.544), (0.389, 0.600), (0.350, 0.636), (0.324, 0.658), and (0.310, 0.668), respectively. Therefore, the emission color of Er^{3+} can be adjusted from yellow–green to green by increasing the pump power, shown as points A_1–A_5 in Fig. 6.

Fig. 7 shows the UC emission spectrum of CPO:0.15Yb^{3+}, 0.006Tm^{3+}, and 0.156Na$^+$ under DL excitation of 980 nm at the pump power of 370 mW. The blue and red emissions around 476, 650, and 700 nm could be ascribed to $^1G_4$–$^3H_6$, $^1G_4$–$^3F_4$, and $^1G_4$–$^3H_5$ transitions of Tm^{3+}, respectively [9,24]. Behind 750 nm, a rather strong emission peak centered at 804 nm is observed, assigned to $^3H_4$–$^3H_6$ transition of Tm^{3+} [9]. Similarly, the dependences of UC emission intensity (476 and 804 nm) on excitation power in this sample were measured and shown in the inset of Fig. 7. The n values for blue and NIR emissions are obtained to 2.31 and 1.58, respectively. Hence, three-photon process is mainly responsible for blue UC and two-photon for NIR UC. Nevertheless, the blue emission presents a much lower experimental value than $n=3$, attributed to two probable reasons as follows. One is similar to that of Er^{3+} (as discussed above). The other is that another UC mechanism related to cooperative UC may be involved. For this type of UC process, the $^1G_4$ energy level of Tm^{3+} is populated via ET from two adjacent Yb^{3+}, which absorb two NIR photons and form a coupled state under the laser pumping, then transfer the energy to $^1G_4$ level of Tm^{3+} [28]. Cooperative UC is a two-photon process, and this will decrease the n value for the general three-photon blue emission of Tm^{3+}. The CIE chromaticity coordinates of this sample at the pump power of 370 mW are calculated to be (0.189, 0.134), indicating a blue emission (see point B in Fig. 6).

Fig. 7. UC emission spectrum of CPO:0.15Yb^{3+}, 0.006Tm^{3+}, 0.156Na$^+$ under DL excitation of 980 nm, the inset shows dependence of UC emission intensity on excitation powder.
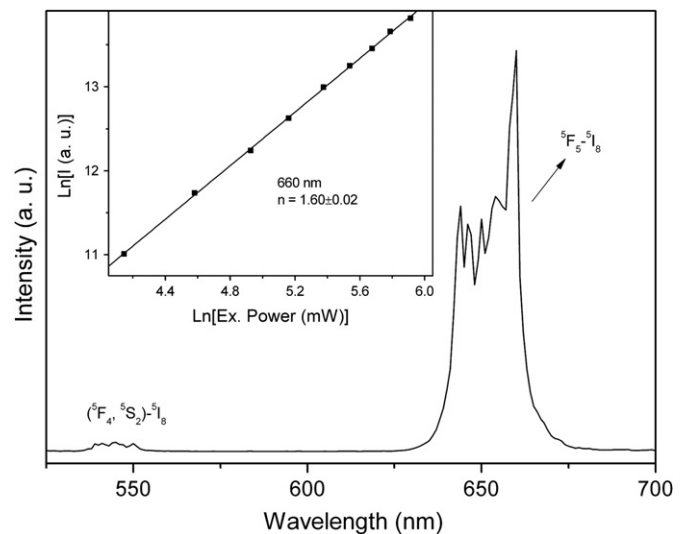
Fig. 8. UC emission spectrum of CPO:0.15Yb^{3+}, 0.03Ho^{3+}, 0.18Na$^+$ under DL excitation of 980 nm, the inset shows dependence of UC emission intensity on excitation powder.

Fig. 8 displays the UC emission spectrum of CPO:0.15Yb^{3+}, 0.03Ho^{3+}, and 0.18Na$^+$ under DL excitation of 980 nm at the pump power of 370 mW. The strong red emission from 625 to 675 nm could be attributed to $^5F_5$–$^5I_8$ transition of Ho^{3+}, and the extremely weak green emission around 545 nm is assigned to ($^5F_4$, $^5S_2$)–$^5I_8$ transition of Ho^{3+} [15]. By fitting the points of UC emission intensity for 660 nm to pump power (see the inset of Fig. 8), we obtained the slope $n=1.60$, which shows the red emission of Ho^{3+} is two-photon process. The CIE chromaticity coordinates of this sample at the pump power of 370 mW are calculated to be (0.692, 0.307), indicating a red emission (see point C in Fig. 6).

For this host, we realize red, green, and blue emissions by co-doping Yb^{3+}–Ho^{3+}, Yb^{3+}–Er^{3+}, and Yb^{3+}–Tm^{3+} in CPO, respectively. Hence, it is a feasible in theory to achieve white-emitting UC phosphor through quadri-doping Yb^{3+}–Ho^{3+}–Er^{3+}–Tm^{3+} in CPO. As Er^{3+} gives a relatively weak emission intensity compared with Ho^{3+} and Tm^{3+} in CPO, we obtained the optimal Er^{3+} doping

Fig. 6. CIE chromaticity diagram with the calculated color coordinates upon 980 nm LD excitation. A_1–A_5 are for CPO:0.15Yb^{3+}, 0.03Er^{3+}, 0.18Na$^+$ at different powers (11.6–480.4 mW), B and C are for CPO:0.15Yb^{3+}, 0.006Tm^{3+}, 0.156Na$^+$ and CPO:0.15Yb^{3+}, 0.03Ho^{3+}, 0.18Na$^+$ at the pump power of 370 mW, respectively; (a) is for CPO:0.15Yb^{3+}, 0.03Er^{3+}, 0.0045Ho^{3+}, 0.005Tm^{3+} at various pump powers.

concentration for CPO:0.15Yb^{3+}, yEr^{3+} to be $y=0.03$ (1 mol% of Ca^{2+}), and by analyzing the relative fluorescence intensities of Er^{3+}, Ho^{3+} and Tm^{3+} when they are separately co-doped with Yb^{3+}, we fix the Er^{3+} and Ho^{3+} contents at 1 and 0.15 mol% of Ca^{2+}, respectively, just vary the Tm^{3+} content. Based on this, a series of CPO:0.15Yb^{3+}, 0.03Er^{3+}, 0.0045Ho^{3+}, xTm^{3+}, (0.1845+x)Na$^+$ (0.003 $\leq x \leq$ 0.009) samples were prepared, and the typical emission spectrum for $x=0.005$ under 980 nm LD excitation with the pump power of 370 mW are presented in Fig. 9. The four strong emission peaks between 460 and 720 nm could be attributed to the transitions of Tm^{3+}, Er^{3+}, and Ho^{3+} as mentioned above. However, a weak emission peak at 452 nm is also observed in this quadri-doped sample. According to Ref. [24], this emission is due to $^1D_2$–$^3F_4$ transition of Tm^{3+}, but interestingly it is absent in Yb^{3+}–Tm^{3+} co-doped CPO as can be seen in Fig. 7. So one can predict that the introducing of Er^{3+} or Ho^{3+} leads to the appearance of this blue emission, some cross-relaxation processes between Tm^{3+} and Ho^{3+} or Er^{3+} have occurred in Yb^{3+}–Ho^{3+}–Er^{3+}–Tm^{3+} quadri-doped CPO, populating $^1D_2$ energy level of Tm^{3+}. To verify this point, the CPO:0.15Yb^{3+}, 0.03Er^{3+}, 0.005Tm^{3+}, 0.185Na$^+$ and CPO:0.15Yb^{3+}, 0.0045Ho^{3+}, 0.005Tm^{3+}, 0.1595Na$^+$ samples were prepared, and their UC emission spectra under 980 nm LD excitation are presented in the left-hand inset of Fig. 9. The blue emission peak at 452 nm is observed in Yb^{3+}–Er^{3+}–Tm^{3+} tri-doped CPO, but it is absent in Yb^{3+}–Ho^{3+}–Tm^{3+} tri-doped CPO, which indicates the addition of Er^{3+} is responsible for the population on $^1D_2$ energy level of Tm^{3+} in Yb^{3+}–Er^{3+}–Ho^{3+}–Tm^{3+} quadri-doped CPO. The cross-relaxation process between Er^{3+} and Tm^{3+} will be discussed through the energy level diagram below. For CPO:0.15Yb^{3+}, 0.03Er^{3+}, 0.0045Ho^{3+}, 0.005Tm^{3+}, and 0.1895Na$^+$, we have calculated the CIE chromaticity coordinates at various pump powers from 138.0 to 520.8 mW. The results are (0.419, 0.379), (0.390, 0.370), (0.373, 0.365), (0.358, 0.362), (0.351, 0.364) and (0.345, 0.364) for $P=$138.0, 216.0, 292.0, 370.0, 445.6 and 520.8 mW, respectively, shown as (a) in Fig. 6. The change of chromaticity coordinates with P could be interpreted by Eq. (2). As the blue emission at 478 nm is mainly three-photon process, its fluorescence intensity is more sensitive to pump power compared with that of green or red emission, which results in the increase of blue emission intensity

Fig. 10. Schematic representation of the energy level diagram for the Er^{3+}, Tm^{3+}, Ho^{3+}, and Yb^{3+} as well as the proposed UC mechanisms to produce the blue, green, and red up-converted emissions.

more quickly than green and red ones. Good white emission is obtained when the excitation power is around 370 mW, the appearance of this sample under 980 nm LD irradiation with pump power at 370 mW is shown in the right-hand inset of Fig. 9. In addition, using the color coordinates calculated above, the correlated color temperature (CCT) of the mixed upconversion fluorescence can be given by the McCamy empirical formula [29]:

$$CCT = -437n^3 + 3601n^2 - 6861n + 5514.31 \qquad (3)$$

where $n=(x-x_e)/(y-y_e)$ is the inverse slope line, and $x_e=0.3320$ and $y_e=0.1858$. The CCT value for CPO:0.15Yb^{3+}, 0.03Er^{3+}, 0.0045Ho^{3+}, 0.005Tm^{3+}, and0.1895Na$^+$ at the pump power of 370 mW is calculated to be 4579 K, which indicates it is mid-white.

Fig. 10 presents the energy level diagram for Er^{3+}, Tm^{3+}, Ho^{3+}, and Yb^{3+} as well as the proposed UC mechanisms to produce the blue, green, and red up-converted emissions. For Yb^{3+}–Er^{3+} pairs, Yb^{3+} initially absorbs a 980 nm photon from laser source and subsequent transferred the energy to a nearby Er^{3+} populating Er^{3+} at $^4I_{11/2}$ level, a second 980 nm photon or ET from Yb^{3+} can further populate the $^4F_{7/2}$ level of Er^{3+}, afterwards Er^{3+} relaxes nonradiatively to the $^2H_{11/2}$ or $^4S_{3/2}$ or $^4F_{9/2}$ levels, resulting in the green ($^2H_{11/2}$, $^4S_{3/2}$)–$^4I_{15/2}$ and red $^4F_{9/2}$–$^4I_{15/2}$ emissions of Er^{3+}. On the other hand, the $^4F_{9/2}$ level may also be populated from the $^4I_{13/2}$ level of Er^{3+} by absorbing a 980 nm photon or ET from Yb^{3+}, with the $^4I_{13/2}$ state being initially populated via non-radiative $^4I_{11/2}$–$^4I_{13/2}$ relaxation. Hence, all the three emissions (525, 550 and 668 nm) undergo two-photon process. For Yb^{3+}–Ho^{3+} pairs, similar excitation and relaxation processes are involved as can be seen in Fig. 10, producing the green (545 nm) and red (660 nm) emissions. For Yb^{3+}–Tm^{3+} pairs, two and three-photon processes coexist. As Tm^{3+} has no corresponding energy level to absorb the NIR photons directly, laser excitation of Yb^{3+} is only considered [14,30], and Yb^{3+} can transfer the excitation energies to Tm^{3+}, which populates the $^3H_4$ and $^1G_4$ upper energy levels, leading to VIS-NIR emissions of Tm^{3+}. As described above, the blue emission originating in $^1D_2$ energy level of Tm^{3+} is not observed in Yb^{3+}–Tm^{3+} co-doped CPO. This is probably due to the less efficient ET from Yb^{3+} to Tm^{3+} when populating $^1D_2$ energy level from $^1G_4$ energy level of Tm^{3+}. Because the phonon-assisted ET rate ($P(\Delta E)$) can be expressed as [31]

$$P(\Delta E) = P(0)e^{-\alpha \Delta E / h\omega} \qquad (4)$$

where $P(\Delta E)$ represents the probability of ET, $P(0)$ represents the probability when ΔE is zero, α is host constant, ΔE represents the energy gap in the process of ET, and ω represents the highest phonon energy in the material. From this equation, one can find that the energy mismatches (ΔE) in UC processes largely influence the phonon-assisted ET rate, that is, the larger the energy mismatch is,

Fig. 9. UC emission spectra of CPO:0.15Yb^{3+}, 0.03Er^{3+}, 0.0045Ho^{3+}, 0.005Tm^{3+}, 0.1895Na$^+$ under DL excitation of 980 nm, the left-hand inset shows UC emission spectra of CPO:0.15Yb^{3+}, 0.03Er^{3+}, 0.005Tm^{3+}, 0.185Na$^+$ and CPO:0.15Yb^{3+}, 0.0045Ho^{3+}, 0.005Tm^{3+}, 0.1595Na$^+$ under DL excitation of 980 nm, the right-hand inset shows the appearance of this sample under 980 nm LD irradiation with pump power at 370 mW.

the smaller the ET rate will be. The energy mismatch between $^2F_{5/2} \rightarrow {}^2F_{7/2}$ Yb^{3+} and $^1G_4 \rightarrow {}^1D_2$ Tm^{3+} transitions is greater than 3000 cm^{-1} [9], so the final transfer will occur with small probability. However, in Yb^{3+}–Er^{3+}–Tm^{3+} tri-doped or Yb^{3+}–Er^{3+}–Ho^{3+}–Tm^{3+} quadri-doped CPO, the nearly resonant cross-relaxation $^4F_{9/2}$(Er^{3+})$+{}^3H_4$(Tm^{3+})$\rightarrow {}^4I_{15/2}$(Er^{3+})$+{}^1D_2$(Tm^{3+}) (energy mismatch of about 112 cm^{-1}) process is very easy to occur by phonon-assisted ET when the $^3H_4$ state of Tm^{3+} is initially populated via two ET processes from Yb^{3+}. Accordingly, the $^1D_2$ energy level of Tm^{3+} is populated, resulting in the $^1D_2$–$^3F_4$ transition of Tm^{3+} (452 nm).

4. Conclusions

In conclusion, we have prepared RE^{3+} (RE=Tb, Yb, Tm, Er, and Ho) doped CPO by conventional solid-state reaction method. From the excitation spectrum by monitoring at 543 nm, it can be seen that Tb^{3+}-single-doped CPO shows several strong and broad absorption bands from 125 to 250 nm, attributed to host absorption and Tb^{3+} f–d transition. Upon 147 nm excitation, intense green emission of Tb^{3+} with a comparable brightness to the commercial Zn$_2$SO$_4$:Mn^{2+} green phosphor is observed. Upon 980 nm LD excitation, Yb^{3+}, Ho^{3+}, Er^{3+}, and Tm^{3+} doped CPO could produce red, green, and blue colors from Yb^{3+}–Ho^{3+}, Yb^{3+}–Er^{3+}, and Yb^{3+}–Tm^{3+} pairs, respectively. And white light color is achieved in Yb^{3+}–Tm^{3+}–Er^{3+}–Ho^{3+} quadri-doped CPO at the pump power of 370.0 mW. The cross-relaxation process between Er^{3+} and Tm^{3+} is investigated to interpret the presence of $^1D_2$–$^3F_4$ emission of Tm^{3+} in Yb^{3+}–Tm^{3+}–Er^{3+}–Ho^{3+} quadri-doped CPO. Laser power dependence of the upconverted emissions as well as the energy level diagrams are studied to understand the UC mechanisms. In sum, the CPO:Tb^{3+}, Yb^{3+}, Ho^{3+}, Er^{3+}, and Tm^{3+} could be potential phosphors as either VUV or upconversion luminescence materials.

Acknowledgments

References

[1] G. Blasse, B.C. Grabmaier, Luminescent Materials, Springer-Verlag, Berlin, Heidelberg, 1994.
[2] Z.J. Zhang, J.L. Yuan, X.J. Wang, D.B. Xiong, H.H. Chen, J.T. Zhao, Y.B. Fu, Z.M. Qi, G.B. Zhang, C.S. Shi, J. Phys. D: Appl. Phys. 40 (2007) 1910–1914.
[3] H.B. Liang, Y. Tao, J.H. Xu, H. He, H. Wu, W.X. Chen, S.B. Wang, Q. Su, J. Solid State Chem. 177 (2004) 901–908.
[4] Z.Y. Zhang, Y.H. Wang, J.C. Zhang, Mater. Lett. 62 (2008) 846–848.
[5] J.H. Song, Y. Song, J. Kim, M. Kim, S. Kwon, D. Park, Y. Kim, D. Zang, IMID/IDMC/ASIA Display'08 Digest 34-3 (2008) 1255.
[6] T. Moon, G.Y. Hong, H.C. Lee, E.A. Moon, B.W. Jeoung, S.T. Hwang, J.S. Kim, B.G. Ryu, Electrochem. Solid-State Lett. 12 (2009) J61–J63.
[7] R. Scheps, Prog. Quantum Electron. 20 (1996) 271–358.
[8] F. Auzel, Chem. Rev. 104 (2004) 139–173.
[9] L.W. Yang, H.L. Han, Y.Y. Zhang, J.X. Zhong, J. Phys. Chem. C 113 (2009) 18995–18999.
[10] N.K. Giri, D.K. Rai, S.B. Rai, J. Appl. Phys. 104 (2008) 113107-5.
[11] W. Lü, X. Ma, H. Zhou, G. Chen, J. Li, Z. Zhu, Z. You, C. Tu, J. Phys. Chem. C 112 (2008) 15071–15074.
[12] G.Y. Chen, Y. Liu, Y.G. Zhang, G. Somesfalean, Z.G. Zhang, Appl. Phys. Lett. 91 (2007) 133103–133105.
[13] I. Etchart, I.H. andez, A. Huignard, M.B. erard, W.P. Gillin, R.J. Curryd, A.K. Cheetham, J. Mater. Chem. 21 (2011) 1387–1394.
[14] N.Q. Wang, X. Zhao, C.M. Li, E.Y.B. Pun, H. Lin, J. Lumin. 130 (2010) 1044–1047.
[15] L.X. Sun, H. Gong, B.J. Chen, H. Lin, E.Y.B. Pun, J. Appl. Phys. 105 (2009) 106109-3.
[16] I.M. Nagpure, S. Saha, S.J. Dhoble, J. Lumin. 129 (2009) 898–905.
[17] K. Mizuguchi, Y. Fukuda, Radiat. Protect. Dosim. 84 (1999) 301–306.
[18] D. Wang, Y.H. Wang, Mater. Sci. Eng. B 133 (2006) 218–221.
[19] Z.J. Zhang, J.L. Yuan, H.H. Chen, X.X. Yang, J.T. Zhao, G.B. Zhang, C.S. Shi, Solid State Sci. 11 (2009) 549–555.
[20] S. Saito, K. Wada, R. Onaka, J. Phys. Soc. Jpn. 37 (1974) 711–715.
[21] H.B. Liang, Y. Tao, Q.H. Zeng, H. He, S.B. Wang, X.Y. Hou, W. Wang, Q. Su, Mater. Res. Bull. 38 (2003) 797–805.
[22] W.H. Di, X.J. Wang, B.J. Chen, H.S. Lai, X.X. Zhao, Opt. Mater. 27 (2005) 1386–1390.
[23] J.D. Liu, Y.H. Wang, X. Yu, J. Li, J. Lumin. 130 (2010) 2171–2174.
[24] J.C. Boyer, L.A. Cuccia, J.A. Capobianco, Nano Lett. 7 (2007) 847–852.
[25] M. Pollnau, D.R. Gamelin, S.R. Luthi, H.U. Güdel, M.P. Hehlen, Phys Rev. B 61 (2000) 3337–3346.
[26] K. Krämer, D. Biner, G. Frei, H. Güdel, M. Hehlen, S. Lüthi, Chem. Mater. 16 (2004) 1244–1251.
[27] X. Bai, H.W. Song, G.H. Pan, Y.Q. Lei, T. Wang, X.G. Ren, S.Z. Lu, B. Dong, Q.L. Dai, L.B. Fan, J. Phys. Chem. C 111 (2007) 13611–13617.
[28] M. Liu, S.W. Wang, J. Zhang, L.Q. An, L.D. Chen, Opt. Mater. 30 (2007) 370–374.
[29] C.S. McCamy, Color. Res. Appl. 17 (1992) 142–144.
[30] Z.G. Xia, W. Zhou, H.Y. Dub, J.Y. Sun, Mater. Res. Bull. 45 (2010) 1199–1202.
[31] R. Reisfeld, C.K. Jørgensen, Laser and Excited States of Rare Earths, New York, 1977.